Experimental results of Multi-Stage Four Quadrant Phase Mask Coronagraph

P. Baudoz[a,b], F. Assemat[a,b], R. Galicher[c], J. Baudrand[a,b], A. Boccaletti[a,b]

[a] LESIA, Observatoire de Paris, CNRS, UPMC, Université Paris Diderot; 5 Place Jules Janssen, 92190 Meudon, France

[b] Groupement d'Intérêt Scientifique PHASE (Partenariat Haute résolution Angulaire Sol Espace) between ONERA, Observatoire de Paris, CNRS and Université Paris Diderot.

[c] LUTH, Observatoire de Paris; 5 Place Jules Janssen, 92190 Meudon, France

ABSTRACT

In the framework of exoplanet direct imaging, a few coronagraphs have been proposed to overcome the large flux ratio that exists between the star and its planet. However, there are very few solutions that gather in the same time broad band achromaticity, a small inner working angle (shortest angular distance for planet detection), a good throughput for the planet light, and a mature technical feasibility. Here, we propose to use a combination of chromatic Four Quadrant Phase Mask coronagraphs to achromatize the dephasing of this well-studied monochromatic coronagraph. After describing the principle of the technique, we present preliminary results for a compact prototype. Contrast larger than 10000 are reached with more than 250 nm of spectral bandwidth in the visible. Stability over time and effect of the filtering is also discussed.

Keywords: High Contrast Imaging, Coronagraphy, Extremely Large Telescope

1. INTRODUCTION

The recent direct discovery of planetary objects orbiting around a few nearby stars is a strong motivation to pursue the development of instrumental techniques to perform direct imaging of exoplanets. Indeed, since these planets have been observed with instruments that were not optimized for such detection, we can expect to learn a lot from dedicated planet finder instrument like SPHERE on the VLT [4] or GPI on Gemini [8], which will be available in a few years. However, these instruments will still be limited mostly to the detection of Jupiter mass planets. We need to wait for the Extremely Large Telescopes (ELT) to be able to detect lower mass planets with direct imaging. This detection is challenging since these planets are much fainter and angularly closer to their host star. The direct imaging of large rocky planets called super-earths is arising as a major scientific goal for EPICS (Kasper et al., 2008 [7]), the planet finder that will take place on the European Extremely Large Telescopes (E-ELT).

Coronagraphy is a very useful tool that could efficiently contribute to planet direct imaging and characterization by removing or attenuating a large part of the stellar light. However, to reach the detection level of rocky planets, it is mandatory to study and develop coronagraphs more efficient than the one developed so far. Measuring the few photons reflected or emitted by the atmosphere of faint planets like super-earths will require reaching very high contrasts over broad spectral bandwidth. Among the different coronagraphs proposed so far, our group has developed an expertise on a phase-mask coronagraph proposed by Rouan et al. 2000 [11], called four-quadrant phase-mask (FQPM). The capabilities of the FQPM have been studied from a theoretical point of view (Rouan et al. 2000 [11]; Riaud et al. 2001 [9]) and in the lab (Riaud et al. 2003 [10]). Our group is also responsible for the study, manufacture, characterization, and delivery of a set of coronagraphic devices for two instruments: the mid-IR imager of the James Webb Space Telescope (Baudoz et al. 2006 [3]), the SPHERE instrument for the VLT (Boccaletti et al. 2008 [4]). Theoretically and practically, a phase mask coronagraph is able to reach very high contrasts. However, in its simplest versions, such a coronagraph is chromatic since the π phase shift is performed for a single optimized wavelength. We propose to use a combination of chromatic phase mask coronagraphs in series to achromatize the overall dephasing of the coronagraph. After briefly recalling the

Ground-based and Airborne Instrumentation for Astronomy III, edited by Ian S. McLean, Suzanne K. Ramsay, Hideki Takami, Proc. of SPIE Vol. 7735, 773581 · © 2010 SPIE · CCC code: 0277-786X/10/$18 · doi: 10.1117/12.858273

principle of this Multi-Stage Four Quadrant Phase Mask (MS-FQPM) coronagraph, we describe the results obtained on a compact prototype of a MS-FQPM associating three monochromatic FQPMs.

2. PRINCIPLE OF THE MULTI-STAGE FOUR QUADRANT PHASE MASK

The principle of the FQPM has already been described elsewhere [11] and is only quickly recalled here. The focal plane is simply split into four equal areas, two of which are phase-shifted by π. As a consequence, a destructive interference occurs in the relayed pupil, and the on-axis starlight is rejected outside the geometrical pupil. An appropriate diaphragm called Lyot stop filter this stellar light. The π phase shift, introduced through an engraved optical substrate, is intrinsically chromatic. To increase achromaticity of the coronagraph, we propose to use several monochromatic coronagraphs in series. This is the principle of the Multi-Stage Four Quadrant Phase Mask (MS-FQPM) first described in Baudoz et al. 2008 [2]. To understand how MS-FQPM works, we can separate the light that propagates through a single FQPM into two parts. One part of the light is diffracted outside of the geometrical pupil downstream of the coronagraph. The other part of the light is not affected by the coronagraph and cannot be blocked out by a Lyot stop. For a monochromatic FQPM working at its optimized wavelength and with a full circular pupil without phase defects, all the light is diffracted outside of the pupil geometry (Abe et al. 2003 [1]). A Lyot stop with the exact size of the pupil can completely block this light. Departing from the optimized wavelength, there will be a fraction of the light that does not interfere. In the extreme case of an observing wavelength equal to half of the optimized wavelength, the dephasing of the coronagraph is 2π and there is no diffracted light.

Since the amplitude distribution of light that does not destructively interfere is not modified in the pupil plane downstream of the coronagraph, we can propagate the beam in another FQPM coronagraph that is optimized for a different wavelength. This could be done infinitely to increase the achromaticity of the coronagraph. With the number of optical surfaces increasing, the problems related to alignment and non-perfect optics will also increase and a trade-off analysis has to be carried out depending on the expected performance and the system complexity. Depending on the number of implemented stages, the wavelength of each FQPM must be optimized to efficiently attenuate the entire spectral bandwidth. For a single FQPM and for a perfect wavefront, Riaud et al 2003 [10] demonstrated that the total residual flux (Ratio of total intensity of the coronagraphic image to that of the direct image) depends only on spectral bandwidth as : $\pi^2.(\lambda_0/\Delta\lambda)^{-2}/48$ As we add more stages, simulation shows that the total residual flux level varies roughly as $[\pi^2.(\lambda_0/\Delta\lambda)^{-2}/48]^N$ with N the number of stages (Baudoz et al. 2008 [2]). For a typical astronomical bandwidth ($R=\lambda_0/\Delta\lambda=5$), a residual level of 10^{-8} is expected with a multi-stage coronagraph using only 4 FQPMs.

3. PROTOTYPE OF MS-FQPM

The tests of a crude MS-FQPM prototype gave promising results (Baudoz et al. 2008 [2]). However, the optical elements of this device were not optimized (wrong AR coating, wavelengths of the FQPM, and so on). Besides, the optical path was longer than 2.5 m, thus more sensitive to internal turbulence and drift of the position of the several FQPMs. The beam ratio was also very large (F/D=300) compared to what would be expected in a real instrument. Thus, we decided to develop a new prototype to demonstrate the feasibility of a compact MS-FQPM more compatible with observatory environment. Our choice is focused on the combination of 3 stages optimized for a spectral bandwidth of 150 to 250 nm centered around 750 nm. The visible wavelength has been chosen to avoid IR detector issue (high background and low sensitivity for passively cooled detector and vibration for actively cooled arrays). The three wavelengths chosen for the monochromatic FQPM masks are: 690 nm, 740 nm, and 800 nm. Figure 1 presents the expected stellar attenuation in function of the wavelength for this prototype (full line). Dotted curves represent the foreseen attenuation limits if an error of 10 nm is made on each of the optimal central wavelengths of the monochromatic masks.

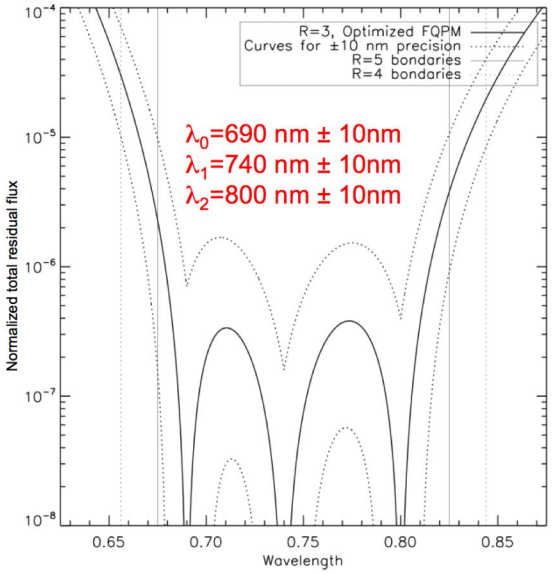

Figure 1 : Residual light diffracted through a perfect MS-FQPM as a function of wavelength. The 3 optimized wavelengths are described in the figure. Dotted lines show the error limit assuming a precision of 10 nm for each wavelength, which is the fabrication precision of our manufacturer.

3.1 Quality of single FQPM

A monochromatic FQPM is manufactured by a deposition or engraving of two opposite quadrants on an optical substrate. At LESIA, we have investigated different materials, several companies and fabrication processes. In the visible wavelength we are interested here, the most natural material is fused silica, which can be either etched or deposited. We manufactured FQPM using both techniques and found relatively identical performance in terms of transition quality and thickness precision. We decided to work with GEPI laboratory because of their proximity (GEPI laboratory is part of Observatoire de Paris as LESIA laboratory) and the fact that they have developed an expertise in fabrication of FQPM. Their precision in thickness reaches 1% of the engraved height, which gives a wavelength precision of roughly 10nm.

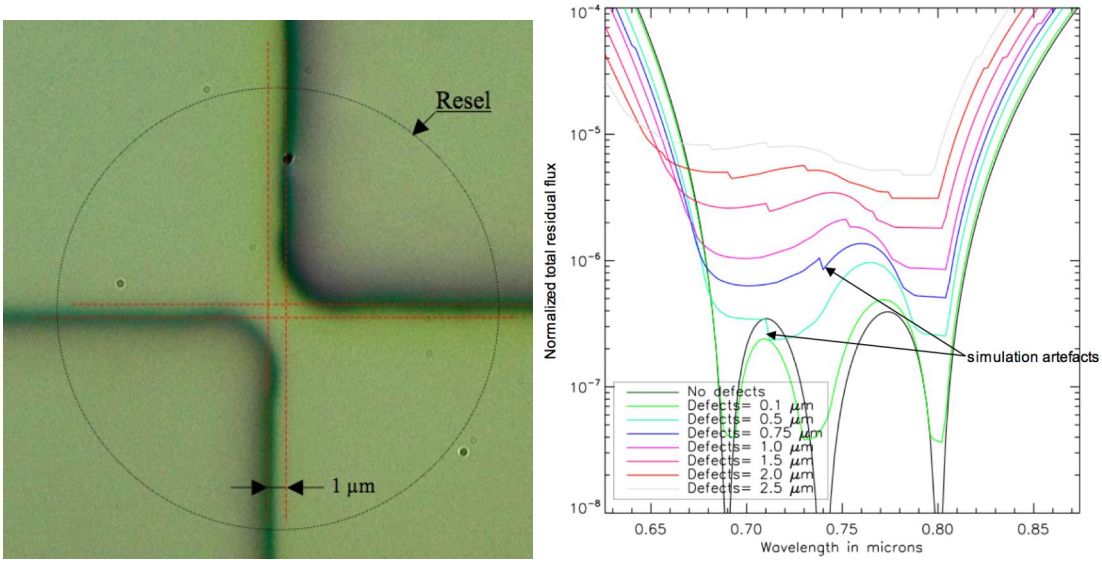

Figure 2. Left: Microscope image of one FQPM transition made by GEPI for this development. Right: Effect of different size defects on the normalized total residual light.

To reach a complete nulling, the transition between the four quadrants must in principle be infinitely small. Departure from this ideal case decreases the attenuation capability of the real FQPM. To compare the effect of different cosmetic

defects, the attenuation is calculated from simulated images. The attenuation varies as a power law of the width defects. The most critical effect is the misalignment of the FQPM transitions, as shown in Figure 2 (left). For this defect, the total residual flux (ratio of total intensity of the coronagraphic image to that of the direct image) can be empirically estimated with the formula 3.33 W_d^2 where W_d is the defect width given in λF/D (Baudoz et al 2006 [3]). A transition precision of roughly 0.5 to 1 μm is reached by GEPI laboratory.

These transition effects will affect more strongly the performance of a coronagraph as the beam ratio and the wavelength decrease. For example, for a given instrument with a F/D=40 and working around 750 nm, a typical defect of 1 μm should limit the performance of a single coronagraph to 300. However, simulation shows that the combination of FQPM mitigates this issue (Figure 2, right). A transition size of 1 μm appears to be enough to reach a residual flux below 10^{-5} for a MS-FQPM made of three FQPMs.

3.2 Pointing precision

The stability in positioning of each FQPM compared to the optical beam is also a crucial element and it has to be taken into account. A simulation shows that each FQPM must be placed on the optical axis with a precision better than 60 nm to avoid decreasing the efficiency of the MS-FQPM. This precision is reached using computer controlled motorized actuators with a 40 nm movement precision. The precision on the Lyot stop positioning is less severe (5 μm in x and y) but still requires movements. With the number of optics increasing, the sensitivity of the device to temperature drift increases. To overcome this effect, we studied a specific mechanical mount made of Invar. The mount of the lenses, the FQPM and the Lyot stop will all be mounted in the same type of mount (Figure 3). Each mount is coupled to the next and previous mount by the mean of 3 posts made of Invar.

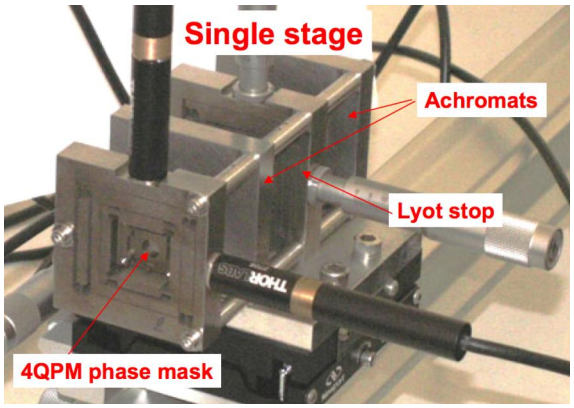

Figure 3: Picture of a single stage

3.3 Opto-mechanical design

The typical optical design of a 3 stages MS-FQPM is shown in Figure 4. The AR coatings of all the elements have been specified and fabricated to value <0.1 % between 650 nm and 850 to avoid the presence of ghosts in the final image.

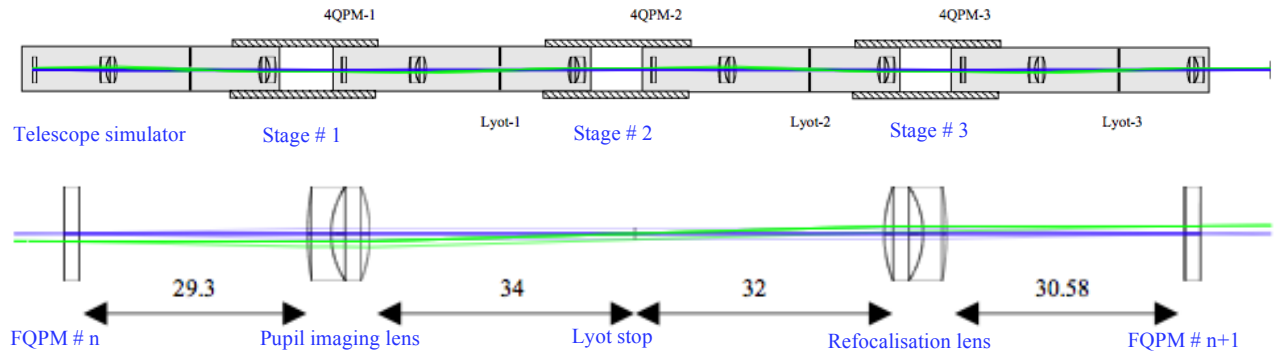

Figure 4 : Up: Optical design for 3 stages. Below: Zoom in of one single stage (distance are in mm)

3.4 Optical setup

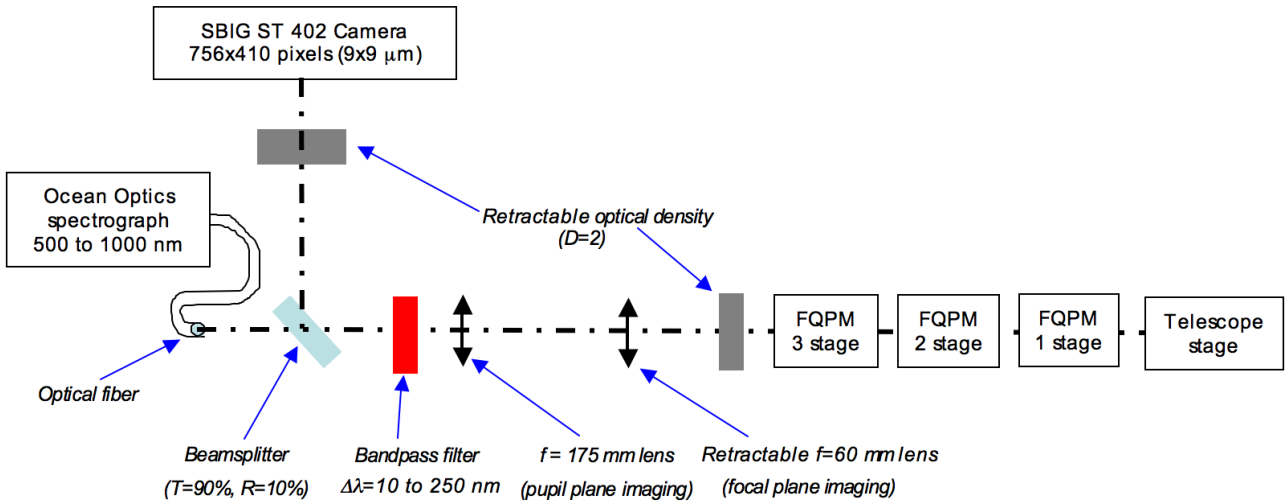

Figure 5 Functional diagram of the MS-FQPM optical test bench

Figure 5 describes the optical setup of the M-FQPM test bench. The light is fed into the telescope stage by a monomode optical fiber connected to a super-continuum fiber laser source (manufacturer : *Fianium*), providing us with a broadband coherent spatial source. Then the light goes through the three coronagraphic stages, each with a FQPM optimized for a specific wavelength, in order to reach high extinction rates. Each coronagraphic stage follows the design described in Section 3.3. The initial pupil (telescope stage) has a diameter of 780 µm. Moreover there is a Lyot filtering in the pupil plane of 90% at each coronagraphic stage, leading to the following characteristics:

- FQPM 1 : pupil with a diameter of 700 µm, FQPM optimized for λ_1=740 nm
- FQPM 2 : pupil with a diameter of 630 µm, FQPM optimized for λ_2=690 nm
- FQPM 3 : pupil with a diameter of 570 µm, FQPM optimized for λ_3=800 nm

The FQPMs are all mounted into the translation stage described in section 3.2, allowing us to move them with a minimal resolution of 40 nm thanks to the servo-motors.

This bench allows us to have either images of the pupil plane or the focal plane on the imaging camera (SBIG ST 402 camera). The camera is conjugated to the pupil plane thanks to a f=175 mm lens. This magnified the pupil image by a factor of 5. An f=60 mm lens can also be inserted into the optical train, providing a focal plane image to measure the characteristics of the image after coronagraphic extinction. In this configuration a beamsplitter allows us to reach an optical fiber (600 µm core diameter), which is linked to a visible spectrograph (manufacturer: Ocean Optics). We can then simultaneously record the focal plane image and the spectrum of the integrated light.

There are two D=2 optical densities on the bench, allowing us not to saturate the detectors when the source is not going through the coronagraphs. These densities are removed when the coronagraphs are aligned on the optical axis, in order to use short exposure times even when the extinction is quite high. The calibration of these densities has been done with great care in order to know precisely the ultimate extinction with all the coronagraphs aligned on the optical axis and the optical densities removed.

We have a set of bandpass filters to restrict the wavelength range from 10nm to 250 nm. The shortest bandwidth are used to characterize the performance of individual FQPMs at their nominal wavelength while the wide band are mandatory to study the chromaticity of the MS-FQPM.

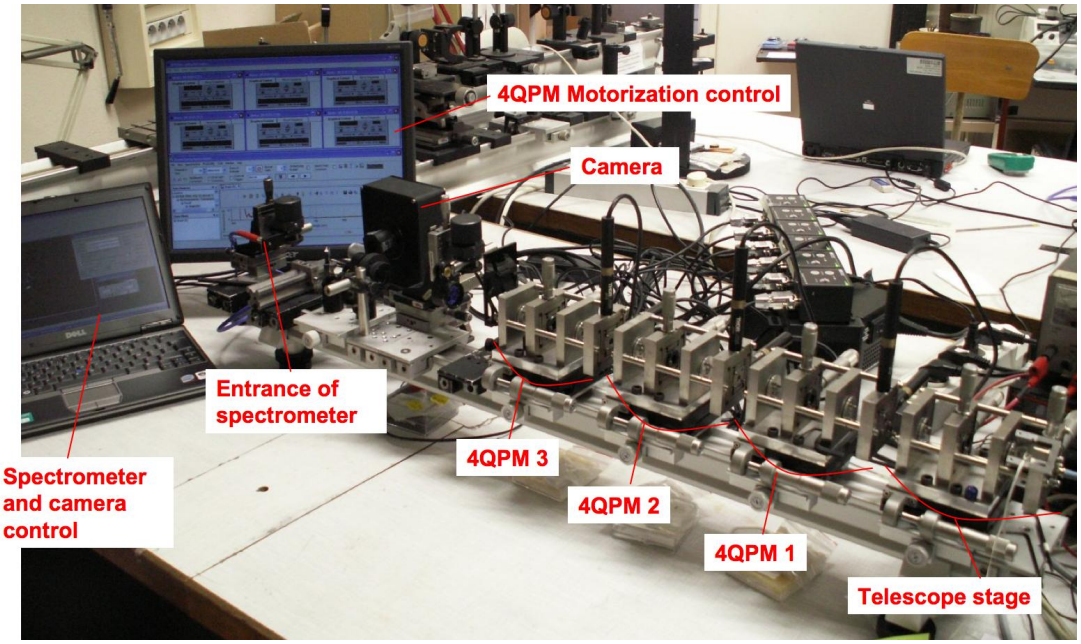

Figure 6 : Photography of the MS-FQPM optical test bench

Figure 6 shows a photograph of the experiment, where we recognize from right to left the telescope stage as well as the three successive coronagraphic stages. The three black cylinders that are visible on each stage are the motorized actuators that move the FQPMs. Three other motors, are also mounted on the horizontal axis. On the left of the figure, we see the camera and the head of the optical fiber that fed the spectrometer. Finally, we can see both computers used to drive the motorized actuators, the camera, and the spectrometer.

3.5 Chromatic behavior

We show in this section the results we have obtained with the MS-FQPM in broadband.

As explained in section 3.4, this bench allows us to have simultaneously the spectroscopic information as well as the spatial information about the coronagraphic image after extinction. In particular a special care was taken for spectra acquisition in order to obtain error bars on the extinction and ensure that we were not dominated by noise, even after very high (>10^4) extinctions, thanks to the acquisition of several spectra and careful calibration of the optical densities.

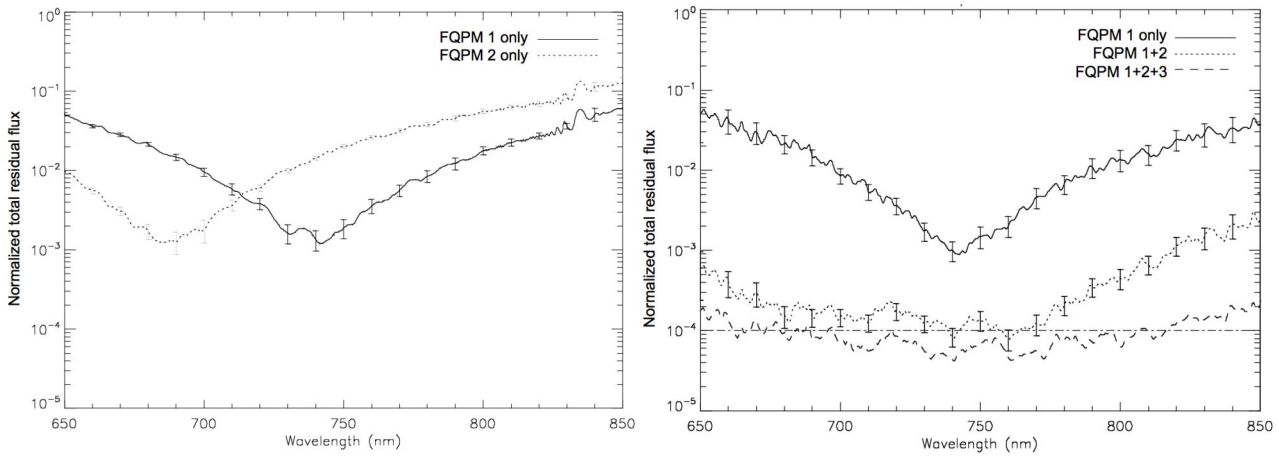

Figure 7 : Evolution of the total residual flux after coronagraphic extinction as a function of the wavelength. Left: for the first and second FQPMs. Right : with 1, 2 and 3 FQPMs aligned on the optical axis (both with logarithmic scale on the vertical axis and normalized with an off-axis source).

The left part of Figure 7 shows the coronagraphic extinction as a function of the wavelength in the case where either the first FQPM (optimized for λ_1=740 nm) or the second FQPM (optimized for λ_2=690 nm) are aligned with the optical axis. We recognize here the classical behavior of a FQPM where the extinction reaches its minimum at the FQPM nominal wavelength. Performance deteriorates rapidly when departing from this optimized wavelength. For instance the nulling for each FQPM reaches a best value of 1000, but it is only equal to a few tenths as soon as there is a difference of 100 nm between the observing wavelength and the nominal wavelength. This well known monochromatic behavior prevents us to achieve high extinction in broad-band imaging with a single FQPM. However, as shown in Figure 7 (right) the serial combination of several FQPMs allows us to definitely increase the performance of the coronagraph on a broad band. With two 4QPMs, one optimized for λ=740 nm and the other for λ=690 nm, the total residual flux is lower than 10^{-3} on a ~200 nm wavelength range. Adding a third FQPM, optimized for λ=800 nm, allows us this time to reach level of 10^{-4} on the same wavelength range.

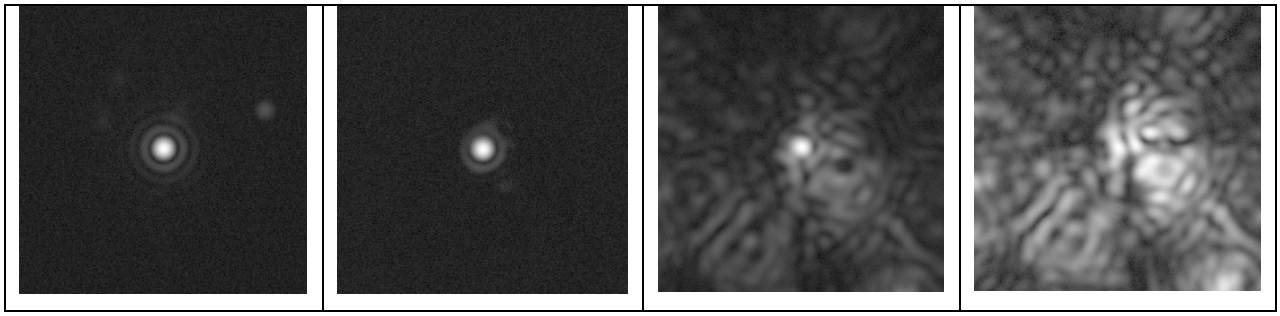

Figure 8 from left to right: non-coronagraphic and coronagraphic image with 1 to 3 FQPMs

The corresponding broad-band images (from 650 nm to 850 nm) are shown on Figure 8. While the intensity of the core of the PSF decreases for each added coronagraph, speckles due to residual aberrations located at a few λ/D seems to have to same shape. These speckles dominate the image when the third coronagraph is aligned with the two other FQPMs.

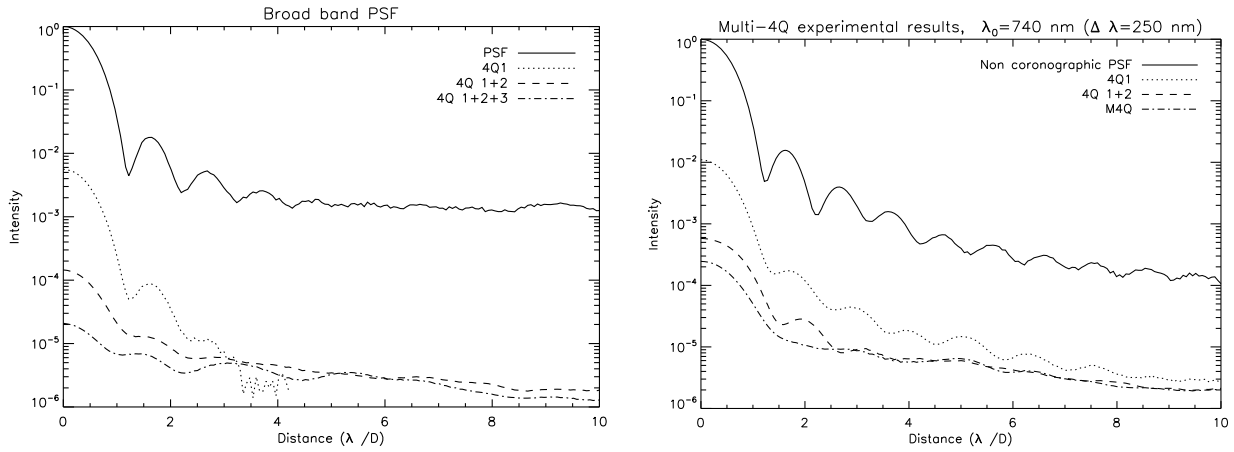

Figure 9 Radial averages of the non-coronagraphic (full line) and coronagraphic images with 1 to 3 FQPMs. Bandwidth : Left: 200nm. Right: 250 nm

Figure 9 shows the radial profiles of the coronagraphic images as a function of the number of the FQPMs inserted into the optical train for two spectral bandwidths: 200 nm and 250 nm corresponding to respectively $\lambda/\Delta\lambda$=3.75, $\lambda/\Delta\lambda$=3. The PSF core is close to 10^{-5} for the shortest bandwidth. The residual intensity on the optical axis increases with the

bandwidth while the level reached at distances further away than 3-4 l/D is similar in both cases. This can be explained by the level of the residual phase and amplitude aberrations and/or ghosts images that are the same for both tests.

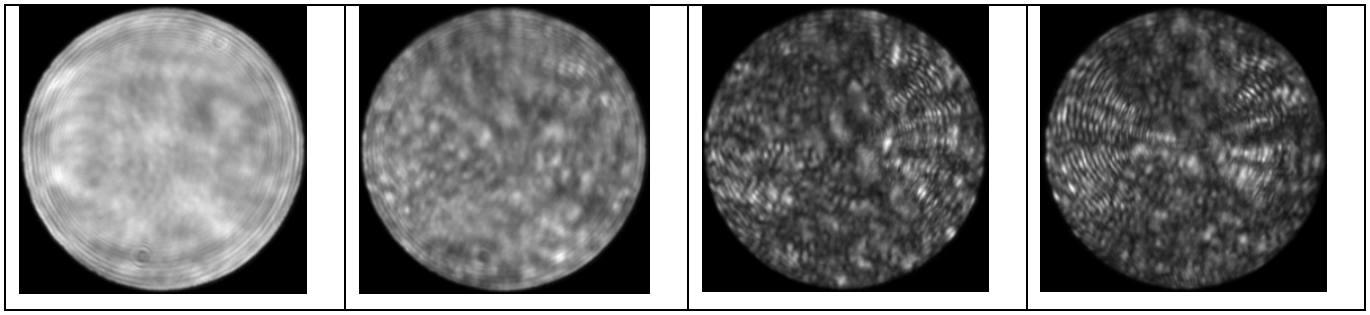

Figure 10 Broad-band pupil images. From left to right : non-coronagraphic and coronagraphic pupils with 1 to 3 FQPMs

Figure 10 shows the pupil images for the different coronagraphic conditions. We can also see here an evolution into the pupil structure and in particular a darkening of the pupil when 3 FQPMs are inserted into the optical train. The pupil image at the end shows a lot of high spatial frequencies structures that may correspond to small-scale defects on the optics.

3.6 MS-FQPM stability over time

The results shown previously were recorded within a small time-scale. However, in practice, such an instrument will be used over long integration times (several hours) in order to detect very faint planets. We have therefore studied the stability over time of the MS-FQPM coronagraph. The results shown in this section were recorded using a spectral resolution R=3 (250 nm bandwidth).

First we aligned the three FQPMs in order to achieve the best nulling. Then we record an MS-FQPM image every 10 minutes for 40 hours. Moreover we measured simultaneously the ambient temperature, knowing that the initial temperature was equal to 19°C. For the first two hours, a heater is started bringing the temperature to 22°C. The heater was then stopped during 14 hours to let the room temperature decrease to 16°C. The heater is then turn up again to reach its maximum temperature (25°C) 24 h after the beginning. The heater was then stopped again until the end of the test.

We measured the stability of the coronagraphic nulling over the time using two criteria:

- Attenuation on the maximum flux into the PSF core (ratio of the maxima of the images on-axis and off-axis of the MS-FQPM)
- Normalized integrated residual flux (ratio of the total flux for the images off-axis and on-axis of the MS-FQPM) but integrated only on a 4 λ/D circular aperture centered on the PSF core.

We observed some variations of the nulling, but this remains quite low. For instance, looking at the attenuation on the maximum flux into the PSF core (Figure 11, left), this one was initially equal to 2.5×10^{-4}, can go as low as 2×10^{-4} (close to the initial nulling), and does not exceed 5×10^{-4},i.e. a factor 2.5 between the best and the worst nulling. We also find the same value for the evolution of the integrated residual flux around the PSF core (Figure 11, right). The changes are really due to a variation of the MS-FQPM performance, as a speckle far from the image center was used for flux calibration in order to correct from some variation of the laser source level, and as an image registration procedure was used to compensate for some slight displacements of the imaging camera. The nulling is the worst for low temperatures (15°C), which is understandable as the initial MS-FQPM was performed at an ambient temperature of 19°C, where in fact we observe the best nulling.

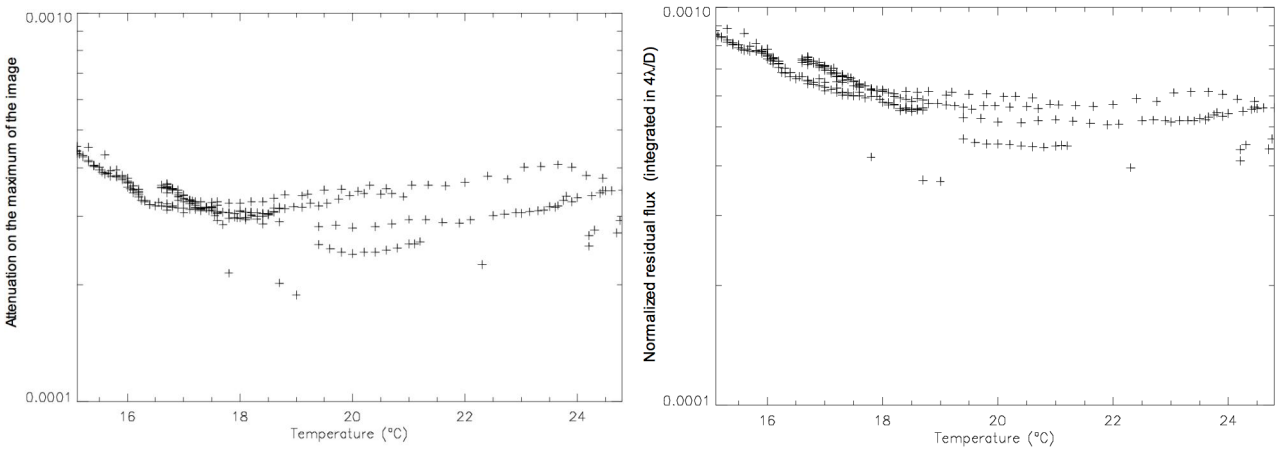

Figure 11: Evolution of the coronagraphic nulling as a function of the ambient temperature. Left : Attenuation on the maximum of the image. Right: Normalized total residual flux integrated into a 4 λ/D circular aperture centered on the PSF core

The data also show that the shape of the residual light in the focal plane is stable with time, meaning that the observed structures have a static behavior, probably because of some ghost image and/or aberrations whose origin remains to be determined.

The MS-FQPM in its current compact configuration provides performance that is quasi-constant with time, thanks to material used for the stages: Invar, which is insensitive to temperature variations. A more detailed study is needed to better estimate the performance of MS-FQPM with time when coupled with the differential spectral imaging techniques that will be needed to detect faint exoplanets.

3.7 Influence of Lyot filtering

The level of Lyot filtering is important in the case of MS-FQPM since as we add more coronagraphs in series, we need to filter the pupil plane with smaller and smaller Lyot stop, which is the opposite of what we want to do to maximize the throughput of the planet light. We used the MS-FQPM test bench to evaluate the impact of the Lyot filtering on coronagraph performance.

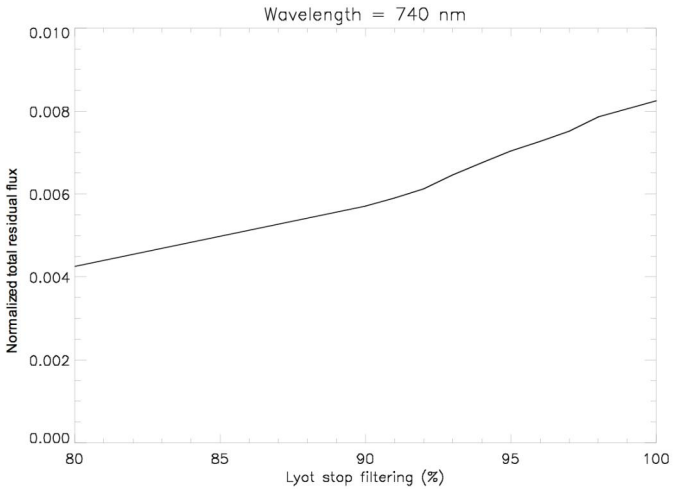

Figure 12 Evolution of the flux extinction (nulling on the total flux on the image) after coronagraphic extinction as a function of the Lyot stop diameter.

Using a single FQPM optimized for 740 nm, we tested several Lyot stop diameters (Figure 12). The data are recorded using a narrow-band filter of 10nm centered on 740 nm. We integrated the flux into the coronagraphic pupil for different diameters and compared it to the initial flux into the full pupil. The result of this study is shown on Figure 12. We

considered a Lyot stop with a diameter going from 80% to 100% of the initial telescope pupil diameter. There is an obvious increase of the flux attenuation with the Lyot stop size, however this increase is very slow. For example, for Lyot stop sizes comprised between 90% and 95%, the nulling for the total flux on the coronagraphic image only goes from $6x10^{-3}$ to $7x10^{-3}$. This increase of the rejection level must be compared to the 15% loss in terms of planet light transmission when changing from 95% to 90% the filtering of the three Lyot stops of the MS-FQPM. These considerations are more important for obstructed pupil because the central obscuration also needs oversizing the central part of the Lyot stop.

We performed the same tests for the two other coronagraphs, where we observed a similar behavior. We intend to study more precisely this effect especially with pupil that have the shape of the European Extremely Large Telescope (obstruction and spiders). Pupil and Lyot stop with 95% filtering are being built and should be tested soon.

4. CONCLUSION

After describing the principle of the Multi-Stage Four Quadrant Phase Mask (MS-FQPM), we have described the compact prototype of MS-FQPM we have built at LESIA. The total length of the instrument is less than 40 cm and can accommodate F/D=40 beam. We have demonstrated the achromaticity of the coronagraph for bandwidth as large as 250 nm ($\lambda/\Delta\lambda=3$). Attenuation as good as 10^{-5} and total integrated residual flux of about 10^{-4} can be achieved in a wide wavelength range ($\Delta\lambda\geq200$nm) with 3 FQPMs, each optimized at a specific wavelength. At this regime, the residual speckles look like the major limitation, justifying post-coronagraphic wavefront sensors as well as a correction of the residual static aberrations thanks to a DM. We have also observed that the extinction remains quasi-constant with time, if low thermal expansion coefficient material (Invar) are used. These results have been obtained with a 90% Lyot filtering at each coronagraphic stage. However we have shown that the coronagraphic performance is not very sensitive to the diameter of the Lyot stop, meaning that 95% Lyot stops could also be used in this configuration. This is very important in terms of detectivity issues, in particular for the case of a realistic telescope aperture with a central obscuration.

Acknowledgments: Part of this work is supported by European Fund Program 7 : E-ELT Prep Phase grant 211257.

REFERENCES

[1] Abe, L., Domiciano de Souza, A., Vakili, F., Gay, J. 2003, A&A, 400, 385
[2] Baudoz, P., Galicher R., Baudrand, J., Boccaletti, A., 2008, Proc. SPIE 7015, 70156C
[3] Baudoz, P. Boccaletti, A., Riaud, P., Cavarroc, C., Baudrand, J., Reess, J.-M., Rouan, D. 2006, PASP, 118, 765
[4] Beuzit J.-L., Dohlen K., Mouillet D., Puget P., Wildi F., Kasper M. et al., 2010, Proc. SPIE 7735
[5] Boccaletti, A., Abe, L., Baudrand, J., Daban J.B., et al., 2008, Proc. SPIE 7015, 70151B
[6] Boccaletti, A., Riaud, P., Baudoz, P., Baudrand, J., Rouan, D., Gratadour, D., Lacombe, F., Lagrange, A.-M., 2004, PASP, 116, 1061
[7] Kasper, M., et al., 2010, Proc. SPIE 7735
[8] Macintosh, B., Graham, J., Palmer, D., Doyon, R. et al., 2008, Proc. SPIE 7015, 701518
[9] Riaud, P., Boccaletti, A., Rouan, D., Lemarquis, F., Labeyrie, A. 2001, PASP, 113, 114
[10] Riaud, P., Boccaletti, A., Baudrand, J., Rouan, D. 2003, PASP, 115, 712
[11] Rouan, D., Riaud, P., Boccaletti, A., Clénet, Y., Labeyrie, A. 2000, PASP, 112, 1479